L_6-X_6 Intervalley Scattering Time and Deformation Potential for $Al_{0.6}Ga_{0.4}As$ Determined by Femtosecond Time-Resolved Infrared Absorption Spectroscopy

W. B. Wang, Kai Shum, and R. R. Alfano

Institute for Ultrafast Spectroscopy and Lasers, Physics and Electrical Engineering Department, The City College and Graduate School of The City University of New York, New York, New York 10031

D. Szmyd and A. J. Nozik

Solar Energy Research Institute, Golden, Colorado 80401

(Received 18 June 1991)

Hot electrons in $Al_{0.6}Ga_{0.4}As$ were produced in the X_6 valley from a photoexcited indirect transition by a 585-nm femtosecond pump pulse. The time evolution of the population of electrons in the bottom of the X_6 valley was monitored by a femtosecond infrared probe pulse. The $L_6 \rightarrow X_6$ intervalley scattering time of ~ 200 fs and the L_6-X_6 intervalley deformation potential of $\sim 2.7\times10^8$ eV/cm were determined from the measured kinetic data.

PACS numbers: 72.10.Di, 72.80.Ey, 78.55.Cr

Intervalley scattering of electrons between conduction-band valleys in bulk or quantum-well semiconductors plays a dominant role in determining the energy relaxation of hot electrons and the high-frequency transport properties of semiconductor devices [1–4]. A large number of experiments have been performed to determine intervalley scattering times such as $t_{\Gamma\rightarrow L}$, $t_{\Gamma\rightarrow X}$, $t_{L\rightarrow\Gamma}$, and $t_{X\rightarrow\Gamma}$ in GaAs [3–6]. As a result of the direct-gap nature and the initial excitation of the Γ-valley electrons rather than the satellite-valley electrons, the L-X intervalley scattering in GaAs cannot be directly monitored, and may be estimated from the L-X intervalley scattering measurement for GaAs alloys such as AlGaAs. However, to our best knowledge, no such measurements have been performed so far. Therefore, the importance of L-X intervalley scattering for the hot-electron relaxation in GaAs has not yet been experimentally revealed.

In this Letter, we present a measurement for $Al_{0.6}Ga_{0.4}As$ using femtosecond visible-pump and infrared-(IR-) probe absorption spectroscopy. The indirect-gap band structure of $Al_{0.6}Ga_{0.4}As$ enables us to eliminate the Γ-valley-involved intervalley scattering and to directly investigate the L_6-X_6 intervalley scattering process [7]. The experimental results yield the first determination of the intervalley scattering time and the deformation potential between the L and X valleys for $Al_{0.6}Ga_{0.4}As$, and give an upper limit of the L-X intervalley scattering time for GaAs.

An undoped 2-μm-thick $Al_{0.6}Ga_{0.4}As$ epilayer sample was grown by the metal-organic chemical-vapor-deposition process in a vertical reactor at a temperature of 725 °C with a growth rate of 12–14 Å/s. The Al content of the sample was determined via electron microprobe analysis and the gas-phase composition measurement with an uncertainty of ± 0.005. The GaAs substrate was completely removed to eliminate the excitation and absorption from the substrate. The steady-state IR transmission spectra of the samples were measured and found to have no appreciable absorption at the probe wavelengths.

A femtosecond visible-pump and IR-probe setup [8] (shown in Fig. 1) was used in this experiment. The output of a Spectral Physics dye laser, pumped by a mode-locked YAG laser (YAG denotes yttrium aluminum garnet) with a fiber-grating pulse-compression and second-harmonic-generation system, was amplified by a pulsed dye amplifier pumped by a Q-switched YAG laser to obtain ~585-nm, ~400-fs pulses. The amplified beam was divided into three parts: One of them was used as a pump to produce hot carriers with a carrier density of 2.8×10^{18} cm^{-3} through a photoexcited indirect transition. The second beam was focused into a methyl alcohol or D_2O cell to generate a white-light continuum which was mixed with the third beam (585 nm) in a $LiIO_3$ crystal to produce IR pulses tuned from 2.5 to 5.5 μm by a difference-frequency method; the latter were used to monitor the induced IR absorption.

The measured time-resolved IR absorption at λ_{probe}

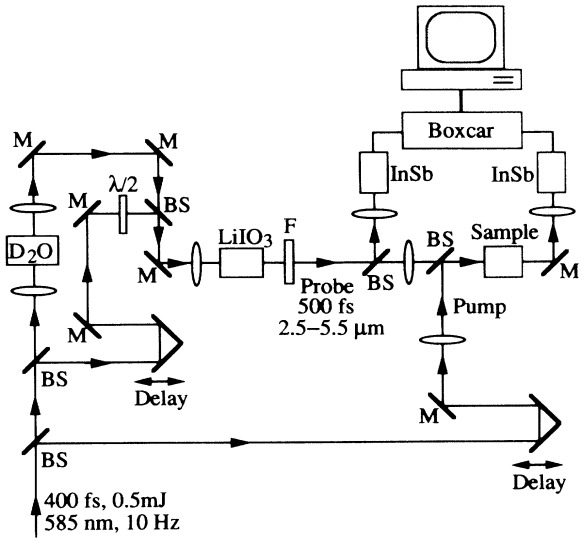

FIG. 1. Femtosecond visible-pump and infrared-probe absorption setup.

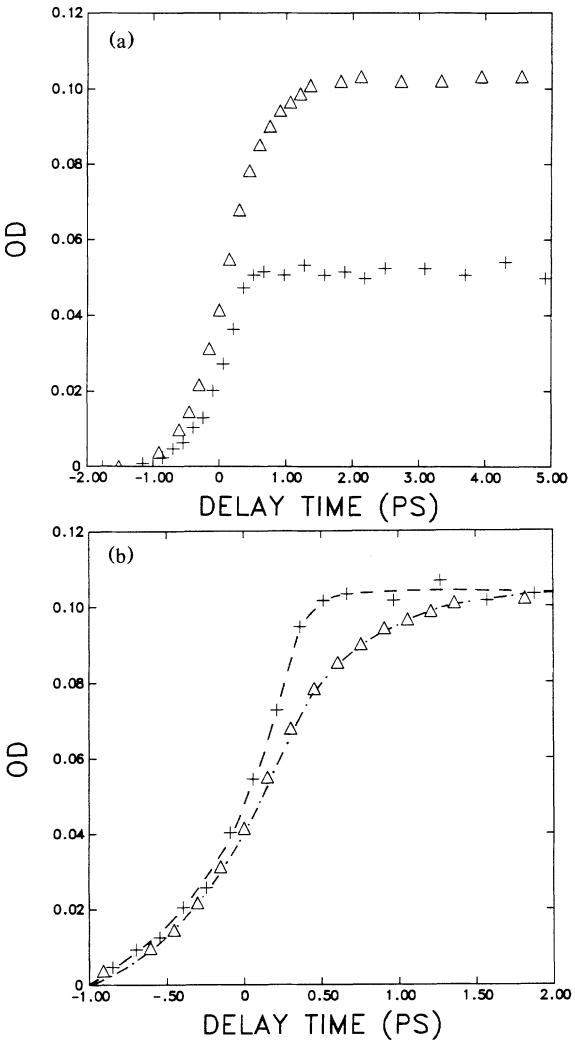

FIG. 2. (a) The measured change in induced optical density at 3.3 (triangles) and 4.0 μm (plusses, $\times \frac{1}{2}$) for $Al_{0.6}Ga_{0.4}As$ at room temperature. (b) The rise portions of both curves in (a) normalized for maximum values.

=3.3 and 4.0 μm for $Al_{0.6}Ga_{0.4}As$ is displayed in Fig. 2(a). The rise parts of these two curves were normalized for their maximum values, and shown in Fig. 2(b). Although the decays of both the curves are flat, the rise time of the 3.3-μm curve is longer than that of the 4.0-μm curve and has two components. To understand the physics behind the differences between the rise times of the two curves in Fig. 2(b), the measurements were extended to other wavelengths between 2.5 and 4.7 μm to obtain the probe-wavelength dependence of the induced IR absorption at a fixed delay time of $t_d = 20$ ps. The measured results are shown in Fig. 3, which indicates an interband transition in the IR region.

An explanation for the induced IR absorption has been discussed previously [9]. The induced total IR absorption is attributed to the following three absorption processes:

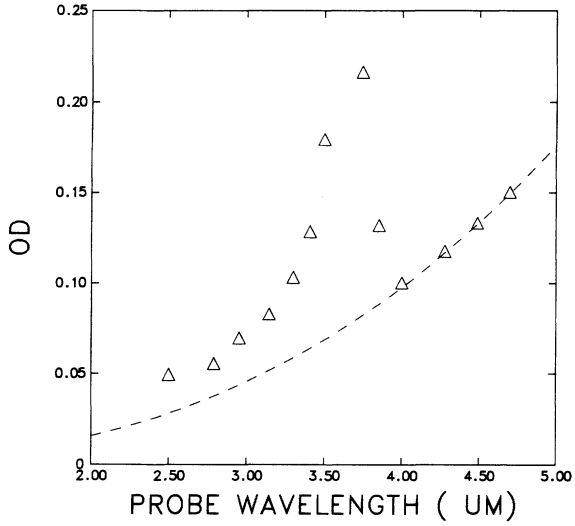

FIG. 3. The probe-wavelength dependence of the induced total IR absorption (triangles) and the free-carrier absorption (dashed line).

(1) inter-conduction-band absorption (ICA) by electrons from the X_6 to the X_7 valleys (see the inset of Fig. 4); (2) inter-valence-band absorption (IVA) by electrons from the split-off to the heavy-hole and light-hole bands and by electrons from the light-hole to the heavy-hold bands; and (3) free-carrier absorption (FCA) by hot electrons in the L and X valleys and by hot holes in the three valence

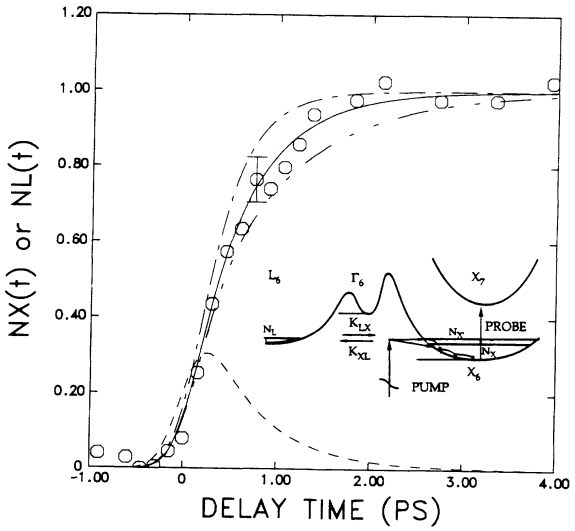

FIG. 4. The time evolution of the population of N_X and N_L. The circles represent the experimental data for N_X. The dot-dashed, solid, and dot-dot-dashed curves are the computer fits for N_X, from rate equations (2)–(4), corresponding to $t_{L\cdot X} = 100$, 200, and 300 fs, respectively. The dashed line is the numerical solution for N_L with $t_{LX} = 200$ fs. Inset: The band structure of the sample, and the relevant scattering processes.

bands.

The calculated optical densities of IVA for $\lambda \geq 3.1$ μm, obtained by using the cross sections for IVA given by Braunstein and Magid [10] and our electron densities in the split-off and the light-hole bands, are less than 0.004, which is much smaller than the observed values shown in Fig. 3. Therefore, IVA can be neglected for $\lambda_{\text{probe}} \geq 3.1$ μm.

The characteristics of FCA can be obtained from Figs. 2 and 3. The absorption for $\lambda_{\text{probe}} \geq 4.0$ μm in Fig. 3 simply increases with probe wavelength and does not show any interband transition structure. This indicates that the energy of the probe photons for $\lambda_{\text{probe}} \geq 4.0$ μm is not sufficient to make transitions for ICA. Consequently, the absorption for those longer wavelengths only arises from FCA. The curve fitting to the data for $\lambda_{\text{probe}} \geq 4.0$ μm using the relation $(\text{OD})_{\text{FCA}} \propto \lambda^n$, and its extension to shorter probe wavelengths, shown in Fig. 3, gives an appropriate value of FCA at each λ_{probe} with the value of $n=2.2$. The temporal behavior of FCA at each λ_{probe}, for example, at $\lambda_{\text{probe}}=3.3$ μm, should be similar to the curve for 4.0 μm in Fig. 2 with its appropriate flat value.

The total IR absorption at 3.3 μm is attributed to both FCA and ICA because a 3.3-μm photon is energetic enough to make the $X_6 \rightarrow X_7$ transitions [9]. Since the temporal behavior of FCA at 3.3 μm should be similar to that at 4.0 μm, the time-resolved $X_6 \rightarrow X_7$ ICA at 3.3 μm, $(\text{OD})_{X_6 \cdot X_7}(t)$, can be obtained by subtracting the FCA curve, $(\text{OD})_{\text{FCA}}(t)$, from the measured total absorption curve, $(\text{OD})_{\text{total}}(t)$.

Since the X_7 states are almost empty, the time-resolved $X_6 \rightarrow X_7$ absorption, $(\text{OD})_{X_6 \cdot X_7}(t)$, obtained by the manner mentioned above, reflects the time evolution of the population of the X_6 electrons, $N_X(t)$. In fact, $N_X(t)$ can be obtained by deconvoluting the transmittance data $T_{X_6 \cdot X_7}(t)$, corresponding to the absorption data of $(\text{OD})_{X_6 \cdot X_7}$, and the probe pulse $I_{\text{probe}}(t)$ using the equation

$$T_{X_6 \cdot X_7}(t_d) = \frac{\int_{-\infty}^{\infty} dt\, I_{\text{probe}}(t-t_d) e^{-N_X(t)\sigma_X d}}{\int_{-\infty}^{\infty} dt\, I_{\text{probe}}(t)}, \quad (1)$$

where $I_{\text{probe}}(t)$ is the instantaneous intensity of the probe pulse assumed to have a Gaussian profile, d is the length of the sample, and σ_X is the $X_6 \rightarrow X_7$ absorption cross section, which can be calculated using the value of $(\text{OD})_{X_6 \cdot X_7}(t)$ in the flat decay region and the carrier density. The deconvoluted result for $N_X(t)$ is shown in Fig. 4.

In contrast with the X-valley electrons having both ICA and FCA, the L-valley electrons only undergo FCA because there are no upper IR active bands for them to undergo ICA. Therefore, the relative IR absorption in the L valley is very small.

The time evolution of the population of the X_6 electrons, $N_X(t)$, was used to extract the value of the $L \rightarrow X$ intervalley scattering time from a rate equation analysis. Electrons excited from the heavy-hole and light-hole bands by 2.12-eV (585 nm) pump photons obtained sufficient energy to reach both the X and L valleys [11] from which they can scatter to each other as well as scatter inside each valley. Although emission and absorption of a phonon increases and decreases the intravalley scattering rate, respectively, both of them increase the intervalley scattering rate [1]. Since the energy of the X minimum (2.023 eV measured from the top of the Γ valence band) is two phonon energies lower than that of the L minimum (2.089 eV), after a few $X \leftrightarrow L$ backward and forward intervalley scatterings, electrons in the L valley will scatter into the X valley and the energy of the electrons in the X valley will decrease to less than 2.089 eV. These electrons in the X valley will then decay to the bottom of the X valley through intravalley scattering.

The rate equations governing the dynamics of the hot carriers through intervalley and intravalley scattering are

$$dN_L(t)/dt = -K_{LX}N_L(t) + K_{XL}N_{X'}(t) + \alpha_L dP(t), \quad (2)$$

$$dN_{X'}(t)/dt = K_{LX}N_L(t) - K_{XL}N_{X'}(t) + \alpha_{X'}dP(t) - K_{XX}N_{X'}(t), \quad (3)$$

$$dN_X(t)/dt = K_{XX}N_{X'}(t) - K_{XV}N_X(t), \quad (4)$$

where $N_L(t)$ is the instantaneous population density of electrons (IPDE) in the L valley; $N_{X'}(t)$ is the IPDE in the X valley whose energies are above 2.089 eV; N_X is the IPDE in the bottom of the X valley; $P(t)$ is the pump photon flux density; $K_{ij}=1/t_{ij}$, for $i,j=L,X$, is the intervalley or intravalley scattering rate shown in the inset in Fig. 4; t_{ij} is the intervalley scattering time from the i to j valley for $i \neq j$; t_{XX} is the average time for the X electrons to undergo an energy loss from above 2.089 eV to the bottom of the X valley by intravalley scattering in the X valley; $K_{XV}=1/t_{XV}$ is the recombination rate of the X electrons and holes in the valence bands, which can be neglected because t_{XV} is much longer than our experimental range of $\sim$50 ps; and α_i $(i=L,X)$ is the absorptance of the sample for the pump pulse at 585 nm.

The rate equations (2)–(4) were solved for $N_X(t)$ numerically by using the Runge-Kutta method. The values of $\alpha_{X'}$ and α_L can be obtained from the steady-state absorption measurement of the sample. The value of t_{XX} and the relationship between t_{XL} and t_{LX} can be obtained using the previously determined intravalley decay constant [12], the intravalley and intervalley scattering theory [1], and the parameters of $m_X=0.766m_0$, $m_L=0.566m_0$, $\varepsilon_{0X}=2.023$ eV, $\varepsilon_{0L}=2.089$ eV, and $\hbar\omega_l=32.94$ meV for $Al_{0.6}Ga_{0.4}As$ [11]. Substituting the above values for the coefficients into the rate equations leaves only t_{LX} unknown, which was treated as a variable parameter to fit the numerical solution for $N_X(t)$ to the experimental data. As examples of fitting, the three curves of the solution of $N_X(t)$ for the three values of $t_{LX}=0.1$, 0.2, and 0.3 ps are shown in Fig. 4. A comparison of the fitting curves with the experimental data gives

a value of $t_{LX}=200$ fs as the best fit. The uncertainty in this determined value t_{LX} was estimated to be $< \pm 100$ fs by considering the experimental error bars and the uncertainty of the parameters used for solving the rate equations.

The time evolution of the population of electrons in the L valley can also be obtained by solving the rate equations (2)–(4) for N_L at a value of t_{LX}. The solution of N_L with $t_{LX}=200$ fs is displayed in Fig. 4 by the dashed curve.

The determined $L \rightarrow X$ intervalley scattering time of $t_{LX}=200$ fs for $Al_{0.6}Ga_{0.4}As$ is attributed to both phonon-assisted (deformation potential related) [1,13] and alloy-disorder-assisted (zero-phonon transition) [14, 15] intervalley scatterings. The recent measurements of Kalt *et al.* [15] show that (1) zero-phonon transitions are efficient in $Al_xGa_{1-x}As$ but negligible in GaAs; (2) in $Al_{0.38}Ga_{0.62}As$, the intervalley scattering time for the alloy-disorder-related transfer, $t_{\rm dis}$, is about 4 times longer than that for phonon-assisted transfer, $t_{\rm phonon}$; and (3) the effect of the disorder for higher x values can be estimated using the simplified formula $1/t_{\rm dis} \propto x(1-x)$. Since the product of $x(1-x)$ is about 2% higher for our sample with $x=0.6$ than that for their sample with $x=0.38$, it is reasonable to choose $t_{\rm dis}$ to be also about 4 times longer than $t_{\rm phonon}$ for $Al_{0.6}Ga_{0.4}As$. The total $L \rightarrow X$ intervalley scattering time t_{LX} can be expressed by the equation of $1/t_{LX}=1/(t_{\rm phonon})_{LX}+1/(t_{\rm dis})_{LX}$. Substituting the relation $(t_{\rm dis})_{LX}=4(t_{\rm phonon})_{LX}$ and the determined value of $t_{LX}=200$ fs into this equation yields the value of $(t_{\rm phonon})_{LX}=250$ fs for $Al_{0.6}Ga_{0.4}As$.

This phonon-assisted $L \rightarrow X$ intervalley scattering time $(t_{\rm phonon})_{LX}$, can be used to determine the deformation potential between the L and X valleys from the equation [1,13]

$$\frac{1}{t_{ij}}=\frac{D_{ij}^2 N_j m_j^{3/2}}{2^{1/2}\pi\hbar^3\rho\omega_{ij}}[(N_{ij}+1)(\varepsilon-\hbar\omega_{ij}-\varepsilon_{0j})^{1/2} + N_{ij}(\varepsilon+\hbar\omega_{ij}-\varepsilon_{0j})^{1/2}], \quad (5)$$

where t_{ij} is the phonon-assisted intervalley scattering time of electrons from the initial ith valley with energy ε to the final jth valley, N_j the number of equivalent valleys (1 for Γ, 3 for X, and 4 for L), m_j the effective mass of electrons in the jth valley, ρ the density of the crystal, $\hbar\omega_{ij}$ the phonon energy for the $i \rightarrow j$ intervalley scattering, N_{ij} the number of intervalley scattering phonons, ε_{0j} the energy in the bottom of the jth valley, and D_{ij} the deformation potential between the ith and jth valleys. The first and the second terms in the square brackets represent transitions involving emission and absorption of phonons, respectively. All of the values of the above-mentioned parameters for $Al_{0.6}Ga_{0.4}As$, except D_{ij}, can be obtained from the literature [11] and our experimental conditions. Substituting the known values and the determined value of $(t_{\rm phonon})_{LX}=250$ fs into Eq. (5) yields the value $D_{LX}=2.7\times10^8$ eV/cm.

Zollner, Gopalan, and Cardona [13] have calculated the L-X intervalley deformation potential D_{LX} for GaAs as well as for AlAs. The total D_{LX}, considering all of the possible phonon modes, was calculated to be 3.8×10^8 eV/cm for GaAs and 3.2×10^8 eV/cm for AlAs. These results indicate that D_{LX} in $Al_xGa_{1-x}As$ changes slightly with x. Therefore, the theoretical value of D_{LX} for $Al_{0.6}Ga_{0.4}As$ can be approximately estimated to be 3.44×10^8 eV/cm, which is slightly higher but in good agreement with our experimental value.

Our determined value of $(t_{\rm phonon})_{LX}=250$ fs for $Al_{0.6}Ga_{0.4}As$ can be used to estimate the upper limit of the $L \rightarrow X$ intervalley scattering time t_{LX} for GaAs. Since $(m_X)_{\rm GaAs} > (m_X)_{Al_{0.6}Ga_{0.4}As}$ [11] and $(D_{LX})_{\rm GaAs} > (D_{LX})_{Al_{0.6}Ga_{0.4}As}$ [13], $(t_{LX})_{\rm GaAs}$ should be smaller [1] than $(t_{LX})_{Al_{0.6}Ga_{0.4}As}$, that is, $t_{LX} < 250$ fs for GaAs. Comparing this result with the Shah *et al.* determination [3] of $t_{L\Gamma}=2.0$ ps shows that $t_{LX} \ll t_{L\Gamma}$ in GaAs. Therefore, electrons scatter back and forth between the L and X valleys more frequently than between the L and Γ valleys. Consequently, the L-X intervalley scattering is more efficient to control the rate of energy relaxation of the energetic hot electrons in the Γ valley for GaAs and more important for high-speed hot-carrier devices.

We would like to thank Dr. L. Rothberg of AT&T for his help in generating IR pulses and Dr. N. Ockman for his helpful discussions. This research is supported in part by ARO and CUNY Organized Research.

[1] E. M. Conwell and M. O. Vassell, IEEE Trans. Electron Devices **13**, 22 (1966).
[2] K. Berthold, A. F. J. Levi, J. Walker, and R. J. Malik, Appl. Phys. Lett. **54**, 813 (1989).
[3] J. Shah, D. Deveaud, T. C. Damen, W. T. Tsang, A. C. Gossard, and P. Lugli, Phys. Rev. Lett. **59**, 2222 (1987).
[4] D. N. Mirlin, I. Ya. Karlik, and V. F. Sapega, Solid State Commun. **65**, 171 (1988).
[5] A. Katz and R. R. Alfano, Appl. Phys. Lett. **53**, 1065 (1988).
[6] W. B. Wang, N. Ockman, M. Yan, and R. R. Alfano, Solid-State Electron. **32**, 1337 (1989).
[7] Since the subscript for all of the bands under discussion is labeled 6, this 6 will be deleted from here on unless noted otherwise.
[8] T. M. Jedju and L. Rothberg, Appl. Opt. **27**, 615 (1988).
[9] W. B. Wang, N. Ockman, M. A. Cavicchia, and R. R. Alfano, Appl. Phys. Lett. **57**, 395 (1990).
[10] R. Braunstein and L. Magid, Phys. Rev. **111**, 480 (1958).
[11] Sadao. Adachi, J. Appl. Phys. **58**, R1 (1985).
[12] J. A. Kash, J. C. Tsang, and J. M. Hvam, Phys. Rev. Lett. **54**, 2151 (1985).
[13] S. Zollner, S. Gopalan, and M. Cardona, Appl. Phys. Lett. **54**, 614 (1989).
[14] A. N. Pikhtin, Fiz. Tekh. Poluprovodn. **11**, 425 (1977) [Sov. Phys. Semicond. **11**, 245 (1977)].
[15] H. Kalt, W. W. Ruhle, K. Reimann, M. Rinker, and E. Bauser, Phys. Rev. B **43**, 12364 (1991).

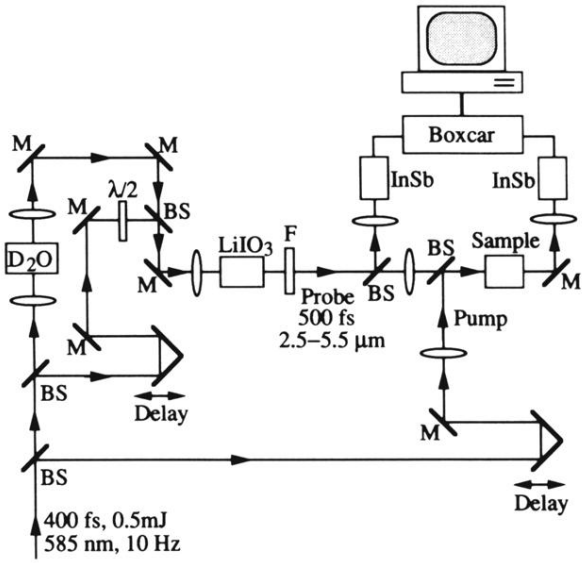

FIG. 1. Femtosecond visible-pump and infrared-probe absorption setup.